Interfacial molecular organization at aqueous solution surfaces of atmospherically relevant dimethylsulfoxide and methane sulfonic acid using sum frequency spectroscopy and computer simulations

Xiangke Chen[1], Babak Minofar[2], Pavel Jungwirth[3], and Heather C. Allen[1*]

[1]The Ohio State University, Department of Chemistry, 100 West 18th Ave, Columbus, OH 43214 USA

[2]Institute of Systems Biology and Ecology of the Academy of Sciences of the Czech Republic and Institute of Physical Biology, University of South Bohemia, Zamek 136, Nove Hrady

[3]Institute of Organic Chemistry and Biochemistry, Academy of Sciences of the Czech Republic, and Center for Biomolecules and Complex Molecular Systems. Flemingovo nám. 2,16610 Prague 6, Czech

Abstract

The molecular organization at the aqueous DMSO and MSA surfaces has been investigated using vibrational sum frequency generation (VSFG) spectroscopy and molecular dynamics (MD) simulations. The molecular orientation of surface DMSO and MSA is deduced based on the VSFG spectra of both C-H stretch and S-O stretch regions. The S-O stretch region is studied for the first time and is shown to be critical in molecular orientation determination. On average, the CH_3 groups of DMSO and MSA are preferentially pointing outwards into the air. However, the DMSO S=O group points slightly inwards away from the surface, while the SO_3 vector of dissociated MSA pointing nearly straight down. In addition, MD simulations reveal that the orientation distribution of surface DMSO is relatively broad in contrast with a narrow distribution of surface MSA, which agrees with the experiment findings.

Introduction

Organosulfur compounds of both natural and anthropogenic origin have been found to be involved in many reactions taking place at the aerosol surface.[1] In the marine boundary layer (MBL), the sulfur cycle dominates in the gas to particle conversion process and in the growth of aerosols.[2] Tropospheric sulfur containing aerosols play an important role in climate as well as in related heterogeneous atmospheric chemical processes.[3, 4] A significant sulfur source in the MBL is the biogenic dimethyl sulfide

(DMS) produced by metabolic processes of algae.[5, 6] Because of its high volatility and reactivity, DMS is easily oxidized in the atmosphere and produces many stable intermediates such as dimethyl sulfoxide (DMSO) and methanesulfonic acid (MSA).[7, 8] Oxidation of DMSO, MSA, and other intermediates can take place at the aerosol surface and in the bulk of the aerosol through reactions with OH radicals, which eventually leads to the formation of H_2SO_4.[9] The sulfur containing aerosols serve as cloud condensation nuclei, influencing the formation of clouds and thereby modifying the earth's albedo.[3, 4, 10] Therefore, the uptake of organosulfur species and the molecular organization at the aerosol surface are of great interest in atmospheric chemistry.

Besides the important atmospheric implications, DMSO, MSA, and their aqueous solutions also have a wide range of applications in other chemical processes. In organic chemistry, DMSO is among the most widely used solvents.[11] Biological properties of DMSO are also important. Due to its amphiphilic nature, DMSO interacts strongly with molecules in cell membranes, which promotes membrane permeability[12, 13] and induces cell differentiation[14] and fusion[15]. Because of its strong interaction with water, aqueous DMSO solution displays strong non-ideal behavior. For example, they can reach freezing points near the temperature of liquid nitrogen, and, therefore, can be used as a cryoprotectant for biological structures such as tissues and proteins.[16] Methanesulfonic acid, similar to DMSO, is completely miscible with water at any concentration. Moreover, MSA is a strong acid (pKa = -1.9) and is widely used as an acid electrolyte in many electrochemical processes.[17]

Extensive efforts have been made to elucidate molecular organization in the bulk solutions of aqueous DMSO and MSA.[18-23] In particular, DMSO-water mixtures have been investigated by a wide variety of experimental techniques such as X-ray and neutron diffraction,[21, 24] infrared (IR) and Raman spectroscopy,[25, 26] nuclear magnetic resonance (NMR),[27, 28] and acoustic spectroscopy[29] as well as computer simulations.[18-20] These studies led to the conclusion that DMSO as a hydrogen bond acceptor forms strong hydrogen bonds with water molecules. The hydrogen bond between DMSO and water is even more pronounced than that between water molecules.[21] The methyl groups of DMSO, although hydrophobic, are loosely hydrated by surrounding water molecules.[27] Similar hydrogen bonding ability of MSA with water is observed due to the S-O moieties.[22]

Because of the noticeable surface preference of DMSO and MSA,[30-32] the structure and properties of the surface of their aqueous solutions are also of interest. In contrast with the relatively abundant bulk information, the molecular organization at the surface is still not well understood due to limited surface-specific techniques for aqueous media. Only nonlinear spectroscopic methods such as second harmonic generation (SHG)[33] and vibrational sum frequency generation (VSFG) have been utilized to study the surface of aqueous solutions of DMSO and MSA.[30-32, 34] A concentration VSFG study of aqueous DMSO showed that the square root of the CH_3

intensity was proportional to the determined surface DMSO number density, which suggested that the average orientation of DMSO CH_3 groups remains unchanged with different mixing ratios with water. However, the actual orientation of DMSO at the surface has not been reported.[34] In addition, a VSFG study calculated the MSA orientation based on the CH_3 symmetric stretch intensities in ssp and sps polarizations. Due to the near zero CH_3 intensity in sps polarization, the determined orientation angle of MSA had a large uncertainty range of 0˚ to 60˚.[32] Computational simulations focused solely on DMSO, showing that this molecule is surface active and oriented at the water surface.[35-37] Thus, a general but not complete picture of the surface of aqueous solutions of DMSO and MSA including the surface concentration, molecular interactions and orientation, and interfacial water structure have been presented.

In this paper, the VSFG technique with complementary infrared (IR) and Raman spectroscopies are employed to present a comprehensive study of the liquid/vapor interface of aqueous solutions of DMSO and MSA to elucidate the molecular organization and orientation, and intermolecular interactions. Taking advantage of the ability to probe in the low frequency vibrational region (fingerprint region), the S-O moieties in DMSO and MSA are investigated here for the first time for these molecules. In concert, molecular dynamics (MD) simulations are performed to gain more insight on the experimental results.

Experimental Section

Materials.

DMSO and methanesulfonic acid (> 99% purity) were purchased from Fisher. 1,2-dipalmitoyl-*sn*-glycero-3-phosphate (DPPA) was obtained from Avanti Polar Lipids (Alabaster, AL). Deionized water (not purged of CO_2) with a resistivity of 18.2 MΩ•cm and a measured pH of 5.5 was from a Barnstead Nanopure system. Concentrations are reported in units of mole fraction denoted as X.

VSFG spectroscopy.

The broad bandwidth VSFG system[38, 39] consists of two 1-kHz repetition rate regenerative amplifiers (Spectra-Physics Spitfire, femtosecond and picosecond versions), both of which are seeded by sub-50 fs 792 nm pulses (the wavelength is tuned for system optimization) from a Ti:sapphire oscillator (Spectra-Physics, Tsunami) and pumped by a 527 nm beam from an all solid-state Nd:YLF laser (Spectra-Physics, Evolution 30). The two regenerative amplifiers provide 85 fs pulses and 2 ps pulses at 792 nm. The spectrally broad femtosecond pulses are used to drive the infrared generation in an OPA (optical parametric amplifier; TOPAS, Quantronix) and then produce broad bandwidth infrared pulses (~200 cm^{-1} FWHM). Stable infrared pulses are tunable in various wavelength regions ranging from 1000 cm^{-1} to 3800 cm^{-1}. The output energy of each 792 nm picosecond pulse was set to 300 μJ, and

the IR energies were ~ 9μJ in the C-H stretching region, and ~ 3μJ in the S-O stretching region at the sample stage.

The intensity of the reflected sum frequency signal, I_{SF}, is proportional to the absolute square of the effective second-order susceptibility, $\chi_{eff}^{(2)}$, and to the visible and IR pulse intensities:[40]

$$I_{SFG} \propto \left|\chi_{eff}^{(2)}\right|^2 I_{vis} I_{IR} \qquad (1)$$

VSFG experiments can be conducted with a variety of polarization combinations of incident visible and IR pulses such as ssp, sps, pss and ppp, where the three polarizations refer to the polarization of sum frequency light, visible light and IR light in order. For instance, ssp means s-polarized output sum frequency signal with s-polarized incident visible and p-polarized incident IR pulses.

In different polarization combinations the effective second-order susceptibility, $\chi_{eff}^{(2)}$ is related to the macroscopic second-order susceptibility $\chi_{ijk}^{(2)}$:[40]

$$\begin{aligned}
\chi_{eff,ssp}^{(2)} &= L_{yy}(\omega_{SF})L_{yy}(\omega_{vis})L_{zz}(\omega_{IR})\sin\theta_{IR}\chi_{yyz} \\
\chi_{eff,ppp}^{(2)} &= -L_{xx}(\omega_{SF})L_{xx}(\omega_{vis})L_{zz}(\omega_{IR})\cos\theta_{SF}\cos\theta_{vis}\sin\theta_{IR}\chi_{xxz} \\
&\quad - L_{xx}(\omega_{SF})L_{zz}(\omega_{vis})L_{xx}(\omega_{IR})\cos\theta_{SF}\sin\theta_{vis}\cos\theta_{IR}\chi_{xzx} \\
&\quad + L_{zz}(\omega_{SF})L_{xx}(\omega_{vis})L_{xx}(\omega_{IR})\sin\theta_{SF}\cos\theta_{vis}\cos\theta_{IR}\chi_{zxx} \\
&\quad + L_{zz}(\omega_{SF})L_{zz}(\omega_{vis})L_{zz}(\omega_{IR})\sin\theta_{SF}\sin\theta_{vis}\sin\theta_{IR}\chi_{zzz}
\end{aligned} \qquad (2)$$

where θ_i is the angle of the indicated light to the surface normal and $L(\omega)$ is the Fresnel factor (see Supporting Information).

Molecular orientational analysis.

The capability of quantitative determination of molecular orientation is a significant advantage of VSFG technique compared to other spectroscopic methods. The macroscopic second-order susceptibility $\chi_{ijk}^{(2)}$ is related to the microscopic molecular hyperpolarizability $\beta^{(2)}$ through average molecular orientation. For the symmetric stretch (SS) of C_{3v} groups discussed in this paper, the nonvanishing $\beta^{(2)}$are $\beta_{aac} = \beta_{bbc}$ and β_{ccc}.[41] The relationship between $\chi_{ijk}^{(2)}$ and $\beta^{(2)}$ through can be expressed as follows:[40-42]

$$\begin{aligned}
\chi_{xxz}^{SS} &= \chi_{yyz}^{SS} \\
&= \frac{1}{2}N_s\beta_{ccc}[<\cos\theta>(1+R) - <\cos^3\theta>(1-R)] \\
\chi_{xzx}^{SS} &= \chi_{zxx}^{SS} = \chi_{yzy}^{SS} = \chi_{zyy}^{SS} \\
&= \frac{1}{2}N_s\beta_{ccc}(<\cos\theta> - <\cos^3\theta>)(1-R) \\
\chi_{zzz}^{SS} &= N_s\beta_{ccc}[<\cos\theta>R + <\cos^3\theta>(1-R)]
\end{aligned} \qquad (3)$$

where θ is the tilt angle of the C_{3v} groups to the surface normal and $R = \beta_{aac}/\beta_{ccc}$ is the hyperpolarizability ratio which can be determined experimentally from polarized Raman spectra.

Combining equation (1) to (3) could allow to measure the ratio of effective second-order susceptibilities $\chi_{eff}^{(2)}$ from the VSFG intensity ratio of different polarization combinations, i.e. I_{ssp}/I_{ppp} and then retrieve the orientation angle of C_{3v} groups. The retrieved orientational parameter D, defined as $\langle\cos\theta\rangle/\langle\cos^3\theta\rangle$, is based on the known values of the Fresnel factors, the experiment geometry, and the hyperpolarizability ratio R. In this work, a δ-distribution of the orientation angle is assumed so that $\langle\cos\theta\rangle = \cos\theta$. However, changing the distribution width of θ will result in change of the retrieved average orientation accordingly. Especially, as shown in previous SHG study, the retrieved orientation angle and the distribution width are subjected to a very large uncertainty if the value of the orientational parameter D is close to 1.66. In that case, the apparent orientation angle retrieved is ~ 39°, which is the so-called "magic angle".[43]

For C_{3v} symmetry groups the value of hyperpolarizability ratio R is related to the Raman depolarization ratio ρ by:[42, 44]

$$\rho = \frac{3}{4 + 5\left(\frac{2R+1}{R-1}\right)^2} \qquad (4),$$

where ρ is the ratio of the Raman intensities with polarization perpendicular and parallel to the excitation light. This is measured by the polarized Raman experiment:

$$\rho = \frac{I_{\perp}}{I_{\parallel}} \qquad (5).$$

Only one of the retrieved R values from solving the quadratic equation is physically correct,[45] which can be validated from a polarized VSFG experiment. For molecular groups with C_{3v} symmetry, the value of $R > 1$ is a simple check from the bond additive model.[41]

However, sometimes the VSFG intensity of a specific polarization combination could be very low (for example, the ppp spectrum of DMSO CH_3 is more than 10 fold lower in intensity than the ssp spectrum), which as a result leads to large experimental errors in orientation analysis from a quantitative aspect. The polarization null angle method, as shown in literature,[42, 46] can improve the accuracy of the measured ratio of effective second-order susceptibilities $\chi_{eff}^{(2)}$ and hence accuracy of the determined orientation angle. A detailed description of the polarization null angle method is in the Supporting Information.

Computer simulations.

MD simulations of DMSO or MSA in an aqueous slab were performed. We used a unit cell containing 863 water molecules and 16 DMSO or MSA molecules (corresponding roughly to 1 M (0.02 X)) . The size of the prismatic unit cell was 30 x 30 x 100 Å and 3D periodic boundary conditions were applied.[47] We used a 12 Å cutoff for intermolecular interactions. Long-range Coulomb interactions were accounted for using the particle mesh Ewald procedure.[48] Simulations were run in the NTV canonical ensemble at 300 K. A time step of 1 femtosecond (fs) was employed and all bonds involving hydrogen atoms were constrained using the SHAKE algorithm.[49] All systems were first equilibrated for 500 picosecond (ps), after which a 1 nanosecond (ns) production run followed.

A polarizable force field was employed. For water, we used the POL3[50] water model. For DMSO or MSA we used the general amber force field parameter set.[51] Partial charges were evaluated using the standard RESP procedure employing the Gaussian 03 program[52] and all MD simulations were performed using the Amber 8 program.[53]

Results and Discussion

DMSO at the surface

DMSO-water mixtures have been investigated by various spectroscopic methods including IR, Raman, and VSFG. The S=O moiety is the key part which accounts for the dipolar interactions of DMSO. Figure 1 shows the Raman spectra in S=O stretch region of a series of DMSO-water mixtures. The peak near 950 cm^{-1} is assigned to a rocking mode of DMSO CH_3.[54] For pure DMSO, a broad band peaked at 1043 cm^{-1} is observed for the S=O stretch mode.[26] The asymmetric band shape ranges from 1000 to 1100 cm^{-1} and has a shoulder at ~ 1055 cm^{-1}. This broad shape of S=O stretch shows the existence of different aggregates in pure DMSO. The S=O frequency of DMSO monomer as diluted in carbon tetrachloride was found to be around 1070 cm^{-1}.[54] Because of the negligible interaction between CCl_4 and the DMSO S=O group, this frequency is considered to be unperturbed. In pure DMSO, a strong dipolar interaction was identified between DMSO molecules, leading to formation of DMSO dimers and chain aggregates.[26, 37] Therefore, the peak at 1043 cm^{-1} is assigned to the symmetric stretch of the cyclic DMSO dimer.[26] As the water content increases in the DMSO-water mixtures, a clear red-shift in the S=O stretch frequency is observed, which is generally attributed to the DMSO-water interaction. The concentration dependence of the S=O frequency red-shift was proposed to be correlated with a cluster model (DMSO)x(H_2O)y. When x >> y, as in nearly pure DMSO, the dipolar interaction between DMSO molecules dominates. On the other hand, hydrogen bonding between DMSO and water molecules is more pronounced when y >> x. At 0.66 X DMSO the peak intensity at 1030 cm^{-1} is about the same as that at 1043 cm^{-1},

which indicates the coexistence of DMSO in different chemical environments. Previous MD simulation also suggested the tendency of DMSO and water to preserve their own structural order upon mixing.[18] In rather dilute DMSO solutions (< 0.33 X) the width of the S=O stretch band becomes narrower, suggesting a more similar or homogeneous environment for DMSO. No significant red-shift is found between the 0.1 X and 0.02 X DMSO solution spectra, both showing the S=O frequency centered at 1012 cm^{-1}.

Although IR activity of the DMSO S=O stretch is also observed (data not shown), VSFG of the DMSO S=O stretch has not been reported so far. Indeed no VSFG intensity in the S=O stretch region is detected for the 0.1 X DMSO in the ssp polarization combination as shown in Figure 2. VSFG intensity not only relates to the molecular hyperpolarizability, but also to the molecular orientation at the surface and therefore lack of ssp polarization signal could indicate surface disordered DMSO molecules or orientation of the S=O near the plane of the surface. However, the significant VSFG intensity of DMSO methyl groups, discussed below, indicates that disorder is not the reason for lack of VSFG signal. Previous MD simulations have predicted the orientation of the S-O vector at the surface of both neat DMSO[37] and aqueous DMSO solutions.[35] The S-O vector orientation of the top layer of molecules was found to be parallel to the surface of neat DMSO, while at the aqueous DMSO (< 0.2 X) surface, the average S-O vector orientation was predicted to be ~ 30˚ away from the surface plane. Both theoretical results suggest that the S-O vector in DMSO prefers to orient close to the surface, which as a consequence, leads to a vanishing of the ssp VSFG intensity.

After spreading of negatively charged phospholipid DPPA onto the 0.1 X DMSO solution, two broad peaks centered at ~ 1012 and ~ 1120 cm^{-1} are observed. The higher frequency peak is the DPPA PO_2^- stretch as shown in Figure 2. The agreement of the 1012 cm^{-1} DMSO peak position with Raman spectra further proves that the lower frequency 1012 cm^{-1} peak is the S=O stretch of DMSO. This result clearly shows that the S-O vector orientation is affected by the local electric field created by the negative charge of the DPPA headgroup at surface, namely the S-O vector is more perpendicular to the surface with the oxygen pointing to the bulk as shown in Scheme 1. This result indicates that an applied field can orient the S=O, and that this orientation can be detected. This result still does not clarify the S=O orientation at the surface of an aqueous solution, but at the least, it excludes the possibility of a rather straight down conformation of the S=O bond.

For DMSO, the two CH_3 groups are in a fixed molecular geometry, $\angle$C-S-C = 97.4˚, and the angle between the S=O bond and the C-S-C plane is 64˚.[35] However, the tilt angle of the CH_3 groups to the surface normal are determined by the angle between the surface normal and the C-S-C plane. Without knowing of the angle between the surface normal and the C-S-C plane, retrieval of DMSO CH_3 orientation angle is not unique.[42] Here we assume the C-S-C plane of DMSO to be perpendicular to the liquid

surface, which leaves the S-O vector to be ~ 26˚ buried close to the surface as suggested by the MD simulation and our VSFG S=O result. The VSFG spectra in the C-H stretch region of 0.2 X DMSO is shown in Figure 3. In ssp polarization the peak centered at 2913 cm^{-1} is the CH_3 symmetric stretch.[30] This single peak has contribution from both CH_3 groups. Here we also assume that the orientation remains relatively constant at all concentrations studied as suggested by the previous concentration study.[34]

Usually the VSFG intensity ratios of different polarization combinations, i.e. ssp, ppp or sps are used to determine the average orientation of the specified group. This method is convenient when appreciable VSFG intensities can be measured in these polarization combinations. For the DMSO CH_3 groups, although there is decent intensity in ssp polarization, intensity in ppp polarization (data not shown) is more than one order of magnitude less than in ssp polarization. Using the VSFG intensity ratio to determine the DMSO CH_3 orientation could therefore be subject to a relatively large error. In this case, the CH_3 orientation can be more accurately determined through polarization null angle analysis as demonstrated in previous studies.[42, 46] In our experiment, the polarization of IR is fixed at p while the polarization of visible is set to - 45˚ (equal mixing of s and p), so that both ssp and ppp VSFG signals can be detected. If the detection polarization angle for VSFG is set to s, only half of the intensity will be observed as shown in Figure 3. A certain detection polarization angle (so called null angle) can be measured at which the total output VSFG intensity vanishes. For 0.2 X DMSO CH_3 groups, the null angle is determined to be -10.8˚ ± 2.0˚ as shown in the inset of Figure 3, which corresponds to the $\chi_{eff,ppp}^{(2)}/\chi_{eff,ssp}^{(2)}$ of -0.191 ± 0.036.

In addition, the value of the hyperpolarizability ratio (R) of DMSO CH_3 groups is required. Because the CH_3 groups are linked to sulfur atoms in DMSO, this R value is different from the terminal CH_3 group in an alkyl chain. One way to experimentally determine the value of R is from the Raman depolarization ratio (ρ), which is 0.03 for DMSO CH_3.[54] As a result, R(CH_3) is calculated using equation (4) to be 2.26.

The two CH_3 groups could have different tilt angles, which can be related through the assumed molecular geometry: $\theta_1 = 97.4^\circ - \theta_2$. Using the values above, the two tilt angles are determined through equations (2) and (3) to be 27.0˚ ± 4.0˚ and 70.4˚ ± 4.0˚, respectively. This indicates that on average, while assuming that the two CH_3 group point toward the air phase, DMSO molecules are only slightly tilted from the surface normal at the surface. However, the above tilt angles of DMSO CH_3 groups are the average values retrieved using a δ-distribution assumption. The orientation parameter D retrieved in our experiment is 1.65 (the value at the magic angle is 1.66), which indicates that the DMSO CH_3 groups could orientate at other average tilt angles, but with relatively broad distributions.[43] Although from the relatively strong CH_3 VSFG signal, the partial ordering of DMSO molecules at the surface is anticipated.

Orientation of DMSO molecules has been also simulated using MD simulations of 1 M DMSO in an aqueous slab. A representative snapshot from the simulation (Figure 4) provides a qualitative flavor of the distribution of DMSO across the slab and about their interfacial orientations. Qualitatively, the density distribution of DMSO molecules averaged over the whole simulation shows the surface activity of this molecule (Figure 5). Results concerning the orientational preference of DMSO are quantified in Figure 6. The x-axis is the orientation angle between the DMSO molecular axis (passing through the carbon and sulfur) and the outward surface normal. A broad distribution of probability is observed for the orientation angle, although it is clear that the overall probability between 0˚ to 90˚ is higher than between 90˚ to 180˚, confirming that on average DMSO CH_3 groups are pointing outward into the air phase. This broad distribution is within the regime as suggested by the value of the determined orientational parameter D. In addition, the maximum probability is found at around 20˚ with a secondary weak maximum around 70˚, supporting the experiment finding of 27.0˚ ± 4.0˚ and 70.4˚ ± 4.0˚ respectively. Hence, in addition to the ordering of the DMSO methyl groups as shown here experimentally and supported by MD simulation, it is concluded that the S=O bond of DMSO is also not disordered, and lies close to the aqueous DMSO solution surface in agreement with a previously reported MD result of the S=O.[35]

MSA at the surface.

Unlike DMSO which can only accept hydrogen bonds, MSA is both a hydrogen bond donor and acceptor. The Raman spectra of aqueous MSA in S-O stretch region are shown in Figure 7. The spectra reveal the sensitivity of the MSA S-O bond frequency to hydration and deprotonation. The difference between the spectra of 0.02 X and pure MSA is marked. A sharp peak at 1050 cm^{-1} is observed at low MSA concentration, which is assigned to the SO_3^- symmetric stretch in the dissociated form.[55] The spectral pattern remains up to 0.1 X MSA concentration, which is in agreement with the over 90% ionization degree of MSA at this concentration as reported in the literature.[55] When the molar ratio of MSA:water is 1:1, undissociated MSA is observed to be dominant. Meanwhile the SO_3^- peak intensity decreases significantly as concentration goes up. The peak at 1126 cm^{-1} and the shoulder around 1174 cm^{-1} are assigned to the bending mode of undissociated S-O-H and the SO_2 symmetric stretch respectively, as suggested by previous studies.[22, 55] Molecular MSA can easily form hydrogen bonds with water and itself.[22] In pure MSA, self association to form cyclic dimers should prevail, while a 1:1 MSA-water complex exists in a 0.5 X MSA solution. However, the Raman peak positions and intensities of the S-O-H bend and SO_2 symmetric stretch are almost identical for pure and 0.5 X MSA regardless of the fact that they are different species. This suggests that the hydrogen bonds formed between MSA molecules and between MSA and water molecules are similar.

Orientation of MSA molecules at the surface is reasonably different for its molecular and ionized forms. At low concentrations (< 0.1 X) MSA molecules dissociate almost

completely and the anion has two co-axial C_{3v} groups, the CH_3 and SO_3^-. Therefore the molecular orientation can be determined from the orientation of either the CH_3 or SO_3^- groups.

The VSFG spectra of 0.1 X aqueous MSA in both C-H stretch and S-O stretch regions are shown in Figure 8. In the C-H stretch region the sharp peak observed at 2944 cm^{-1} is from the symmetric stretch of the CH_3 group. The negative interference feature around 3030 cm^{-1} is the position of the CH_3 asymmetric stretch. The apparent peak positions are not the exact peak positions of the component peaks due to interference of adjacent resonances. In addition, the broad proton continuum intensity is clearly seen to extend down below 2800 cm^{-1}. The VSFG intensities in ppp and sps polarizations, however, are nearly undetectable, which is in accordance with previous reports.[32] Therefore it is not possible to accurately measure the CH_3 orientation based on such low spectral intensities. In contrast, the VSFG intensities of the SO_3^- group in both ssp and ppp polarizations can be collected with relatively good signal-to-noise ratios as shown in Figure 8. Similarly the Raman depolarization ratio $\rho(SO_3^-)$ is measured to be 0.039 ± 0.001 from a polarized Raman experiment (Supporting Information), which then gives the hyperpolarizability ratio $R(SO_3^-)$ of 2.65 ± 0.05. Therefore based on the measured intensity ratio of ssp/ppp and the $R(SO_3^-)$ above, the average tilt angle of SO_3^- group can be determined through equations (2) and (3) to be 16.0˚ ± 2.0˚, indicating a relatively straight up conformation of MSA, aligned with the surface normal.

To check the validity of the orientation angle of SO_3^- group, one can back out this value with the measured C-H stretch intensities. The tilt angle of CH_3 group is the same as the SO_3^- group in dissociated MSA, and as determined here, it is 16˚. In addition, the Raman depolarization ratio and the hyperpolarizability ratio of the MSA CH_3 group are determined to be 0.009 ± 0.001 and 1.49 ± 0.03 (Supporting Information). It is noticeably different between the R value of the CH_3 groups in DMSO and MSA which arises from different molecular structure and electron density. The deduced VSFG intensity ratio of ssp/ppp from the values above is ~ 20 at the 16˚ tilt angle, which in agreement with the fact that the ppp and sps intensities are almost undetectable.

A representative snapshot from the MD simulation result of 1 M (0.02 X) MSA solution is shown in Figure 9. MSA is assumed in its deprotonated (anionic) form. The corresponding density profiles, demonstrating the surface activity of MSA are shown in Figure 10. Finally, the orientational profile of MSA is depicted in Figure 11. The orientation angle of MSA (angle between the sulfur-carbon axis and the outward surface normal) shows an obvious preference between 0˚ to 90˚, indicating that the CH_3 group of MSA molecules is pointing outward with a preference to be aligned near to the surface normal. Moreover, the orientation probability increases continuously from 90˚ to a plateau near 20˚. The most probable region occurs below 20˚ where the probability value peaks at 5˚, which is in accordance with the straight

up conformation deduced from experiment results.

Conclusion

A comprehensive investigation of the molecular organization at aqueous DMSO and MSA surfaces has been completed using VSFG spectroscopy and MD simulations. For DMSO molecules at the aqueous surface, the orientation has a relatively broad distribution, but preferentially with the two CH_3 groups pointing outwards into the air. On average, the two DMSO CH_3 groups are tilted at the surface, with tilt angles of ~ 27° and ~ 70°, respectively. The S=O group is hydrated by the aqueous phase and points only slightly inwards to the interior of the solution. MSA molecules completely dissociate into hydrated ions at low concentrations (< 0.1 X). Deprotonated MSA (methanesulfate anions) reside at the surface in a relatively straight up conformation with their SO_3 vector pointing inward and their CH_3 vector pointing outward, with both moieties oriented ~ 16 degrees from the surface normal in their residing phase, aqueous and gas, respectively.

Acknowledgements
X.C. and H.C.A acknowledge support from the National Science Foundation (NSF-CHE 0749807) for the completion of this work. Support to P.J. the Academy of Sciences (Praemium Academie), the Czech Ministry of Education (grants LC512), and the US-NSF (grant CHE0909227) is gratefully acknowledged.

Supporting Information:
Supporting Information Available: Full description of the material. This material is available free of charge via the Internet at http://pubs.acs.org.

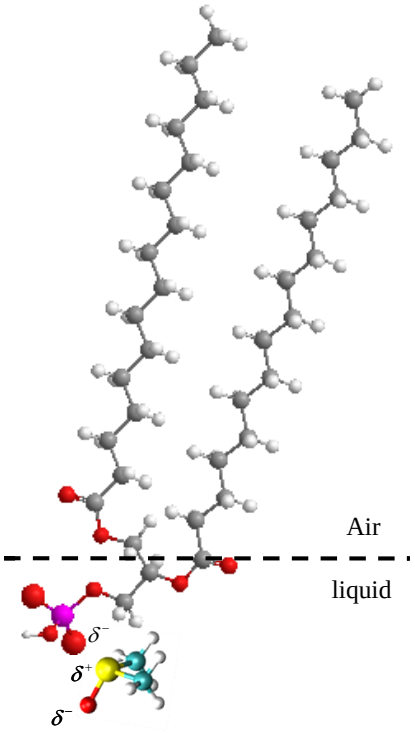

Scheme 1. Influence of DPPA on DMSO orientation at the interface.

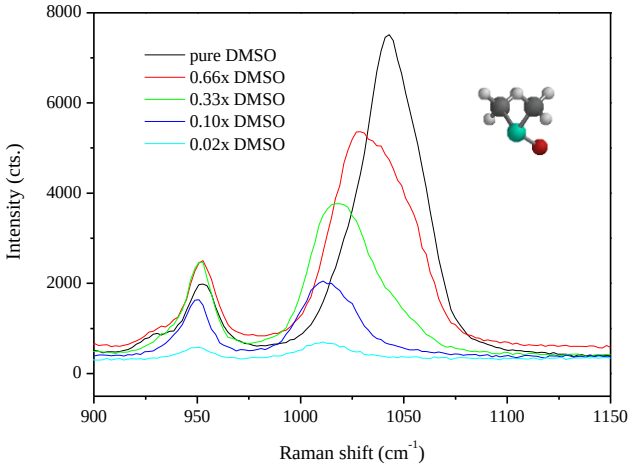

Figure 1. S=O stretch region Raman spectra of a series of DMSO-water mixtures. Structure of DMSO is shown in graph.

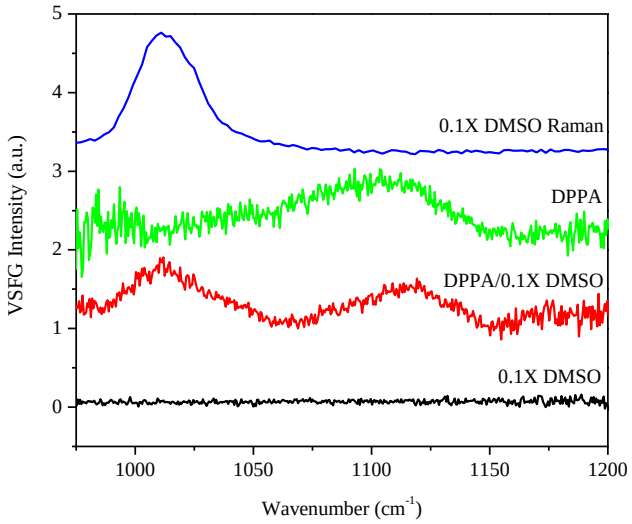

Figure 2. VSFG spectra in S=O region of 0.1X aqueous DMSO. The impact of DPPA on DMSO orientation is shown.

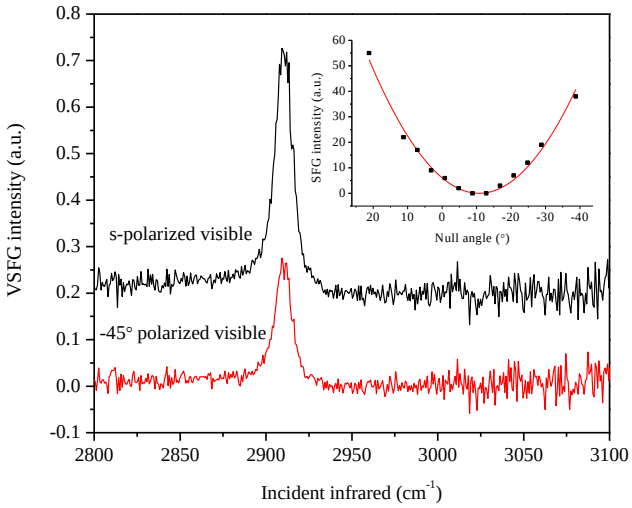

Figure 3. Polarization null angle study of 0.2X aqueous DMSO CH_3 group. The null angle is shown in the inset.

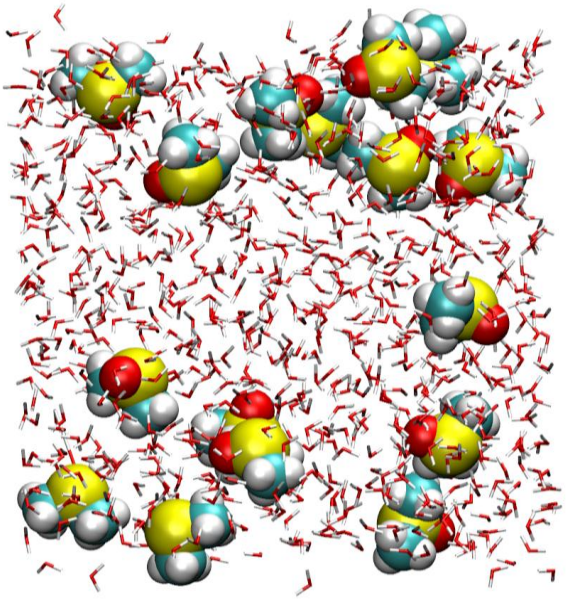

Figure 4. A representative snapshot from the MD simulation of 1 M (0.02 X) DMSO in an aqueous slab.

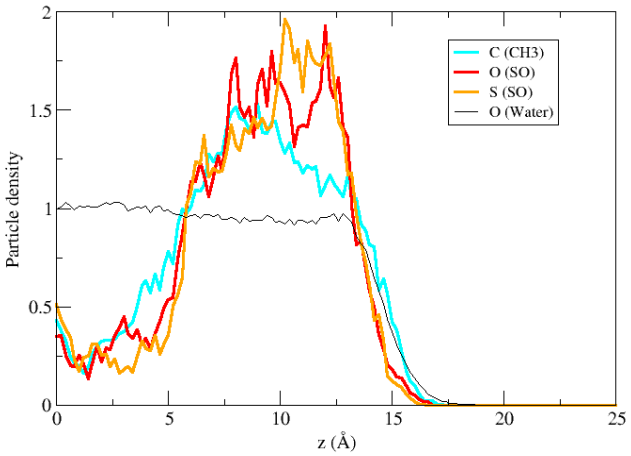

Figure 5. Density profiles of the DMSO molecules from the center of the slab across the water/vapor interface into the gas phase from the MD simulation.

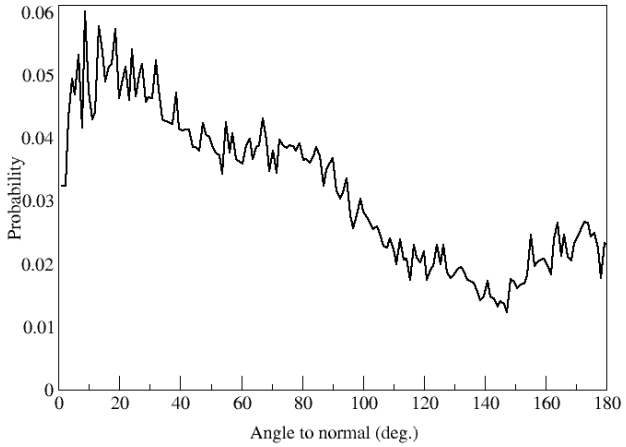

Figure.6. MD simulation of the orientation angle of 1 M (0.02 X) DMSO solution. Orientation angle is defined between the DMSO molecular axis (passing through carbon and sulfur) and the surface outwards normal.

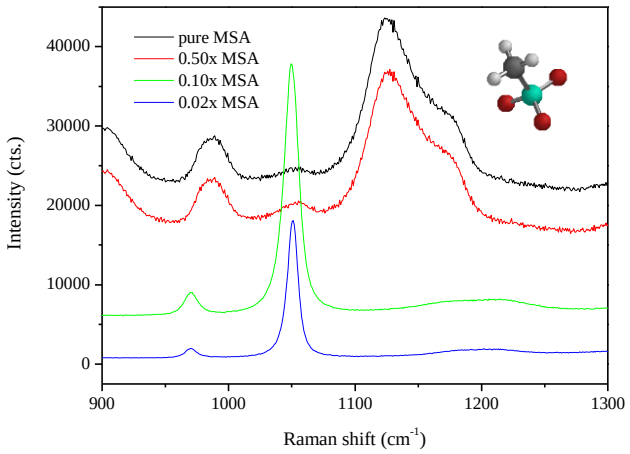

Figure 7. S-O stretch region Raman spectra of a series of MSA-water mixtures. Structure of dissociated MSA is shown in graph.

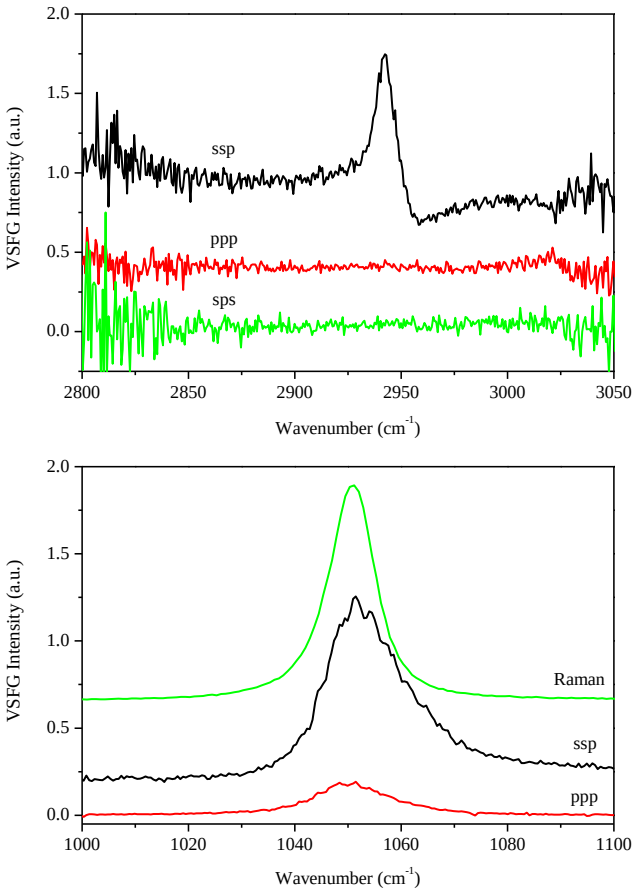

Figure 8. VSFG spectra in both C-H stretch (upper graph) and S-O stretch (lower graph) region of 0.1X aqueous MSA.

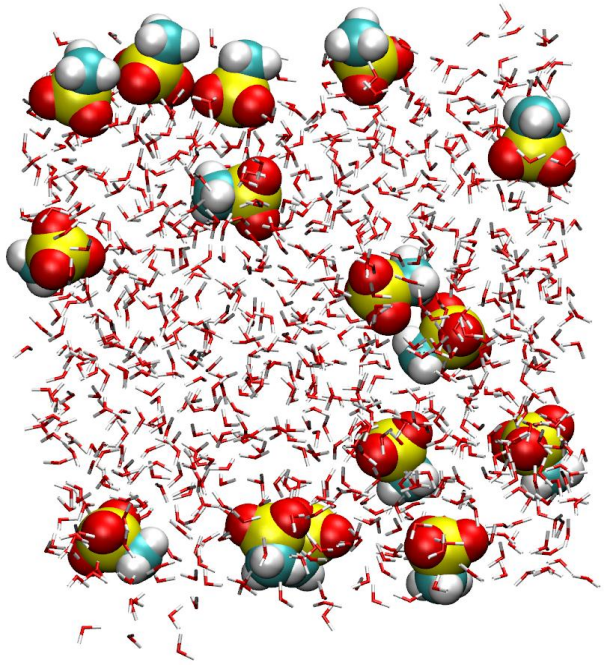

Figure 9. A representative snapshot from the MD simulation of 1 M (0.02 X) MSA in an aqueous slab.

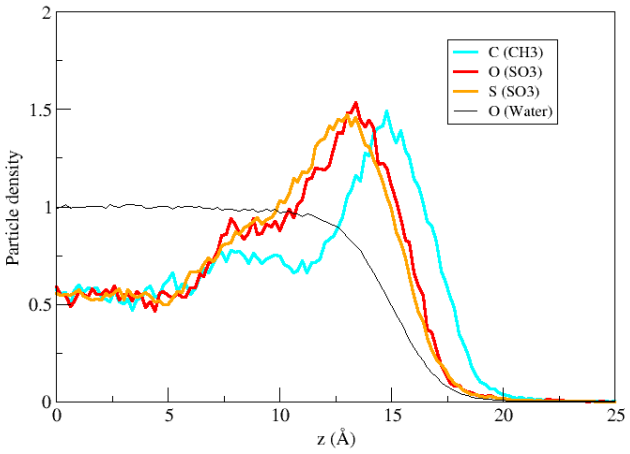

Figure 10. Density profiles of the MSA molecules from the center of the slab across the water/vapor interface into the gas phase from the MD simulation.

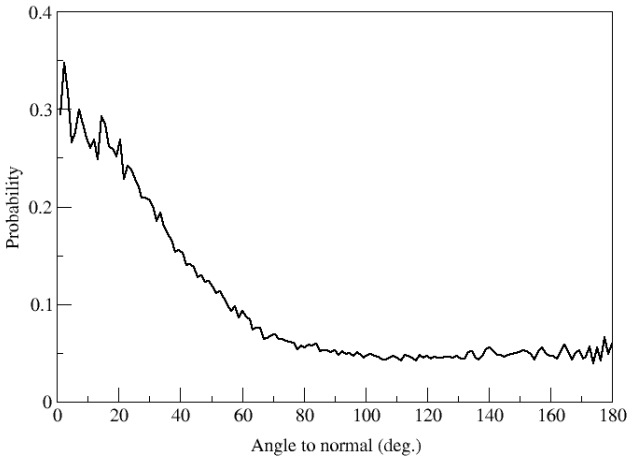

Figure 11. MD simulation of the orientation angle of 1 M (0.02 X) MSA solution. Orientation angle is defined between the MSA molecular axis (passing through the sulfur and the carbon of methyl group) and the surface outwards normal.

References

1. Ellison, G. B.; Tuck, A. F.; Vaida, V., *J. Geophys. Res.-Atmos.* **1999,** 104, 11633-11641.
2. Debruyn, W. J.; Shorter, J. A.; Davidovits, P.; Worsnop, D. R.; Zahniser, M. S.; Kolb, C. E., *J. Geophys. Res.-Atmos.* **1994,** 99, 16927-16932.
3. Charlson, R. J.; Lovelock, J. E.; Andreae, M. O.; Warren, S. G., *Nature* **1987,** 326, 655-661.
4. von Glasow, R.; von Kuhlmann, R.; Lawrence, M. G.; Platt, U.; Crutzen, P. J., *Atmos. Chem. Phys.* **2004,** 4, 2481-2497.
5. Schwartz, S. E., *Nature* **1988,** 336, 441-445.
6. Wakeham, S. G.; Dacey, J. W. H., *Acs Symposium Series* **1989,** 393, 152-166.
7. Yin, F. D.; Grosjean, D.; Seinfeld, J. H., *J. Atmos. Chem.* **1990,** 11, 309-364.
8. Barone, S. B.; Turnipseed, A. A.; Ravishankara, A. R., *Faraday Discuss.* **1995,** 100, 39-54.
9. Schweitzer, F.; Magi, L.; Mirabel, P.; George, C., *J. Phys. Chem. A* **1998,** 102, 593-600.
10. Charlson, R. J.; Schwartz, S. E.; Hales, J. M.; Cess, R. D.; Coakley, J. A.; Hansen, J. E.; Hofmann, D. J., *Science* **1992,** 255, 423-430.
11. Martin, D.; Weise, A.; Niclas, H. J., *Angew. Chem.-Int. Edit.* **1967,** 6, 318-334.
12. Anchordoguy, T. J.; Carpenter, J. F.; Crowe, J. H.; Crowe, L. M., *Biochimica Et Biophysica Acta* **1992,** 1104, 117-122.
13. Barry, B. W., *Nat. Biotechnol.* **2004,** 22, 165-167.
14. Lyman, G. H.; Preisler, H. D.; Papahadjopoulos, D., *Nature* **1976,** 262, 360-363.
15. Ahkong, Q. F.; Fisher, D.; Tampion, W.; Lucy, J. A., *Nature* **1975,** 253, 194-195.
16. Rall, W. F.; Fahy, G. M., *Nature* **1985,** 313, 573-575.
17. Gernon, M. D.; Wu, M.; Buszta, T.; Janney, P., *Green Chem.* **1999,** 1, 127-140.
18. Vaisman, II; Berkowitz, M. L., *J. Am. Chem. Soc.* **1992,** 114, 7889-7896.
19. Soper, A. K.; Luzar, A., *J. Chem. Phys.* **1992,** 97, 1320-1331.
20. Luzar, A.; Chandler, D., *J. Chem. Phys.* **1993,** 98, 8160-8173.
21. Soper, A. K.; Luzar, A., *J. Phys. Chem.* **1996,** 100, 1357-1367.
22. Givan, A.; Loewenschuss, A.; Nielsen, C. J., *J. Mol. Struct.* **2005,** 748, 77-90.
23. Li, S. J.; Qian, W.; Tao, F. M., *Chem. Phys. Lett.* **2007,** 438, 190-195.
24. Bertagnolli, H.; Schultz, E., *Ber. Bunsen-Ges. Phys. Chem. Chem. Phys.* **1989,** 93, 88-95.
25. Brink, G.; Falk, M., *J. Mol. Struct.* **1970,** 5, 27-30.
26. Bertoluzza, A.; Bonora, S.; Battaglia, M. A.; Monti, P., *J. Raman Spectrosc.* **1979,** 8, 231-235.
27. Mizuno, K.; Imafuji, S.; Ochi, T.; Ohta, T.; Maeda, S., *J. Phys. Chem. B* **2000,** 104, 11001-11005.
28. Catalan, J.; Diaz, C.; Garcia-Blanco, F., *J. Org. Chem.* **2001,** 66, 5846-5852.
29. Kaatze, U.; Brai, M.; Scholle, F. D.; Pottel, R., *J. Mol. Liq.* **1990,** 44, 197-209.
30. Allen, H. C.; Gragson, D. E.; Richmond, G. L., *J. Phys. Chem. B* **1999,** 103, 660-666.

31. Allen, H. C.; Raymond, E. A.; Richmond, G. L., *Curr. Opin. Colloid Interface Sci.* **2000,** 5, 74-80.
32. Allen, H. C.; Raymond, E. A.; Richmond, G. L., *J. Phys. Chem. A* **2001,** 105, 1649-1655.
33. Karpovich, D. S.; Ray, D., *J. Phys. Chem. B* **1998,** 102, 649-652.
34. Tarbuck, T. L.; Richmond, G. L., *J. Phys. Chem. B* **2005,** 109, 20868-20877.
35. Benjamin, I., *J. Chem. Phys.* **1999,** 110, 8070-8079.
36. Senapati, S., *J. Chem. Phys.* **2002,** 117, 1812-1816.
37. Darvas, M.; Pojjak, K.; Horvai, G.; Jedlovszky, P., *J. Chem. Phys.* **2010,** 132, 134701-10.
38. Hommel, E. L.; Allen, H. C., *Anal. Sci.* **2001,** 17, 137-139.
39. Tang, C. Y.; Allen, H. C., *J. Phys. Chem. A* **2009,** 113, 7383-7393.
40. Zhuang, X.; Miranda, P. B.; Kim, D.; Shen, Y. R., *Phys. Rev. B* **1999,** 59, 12632-12640.
41. Hirose, C.; Akamatsu, N.; Domen, K., *J. Chem. Phys.* **1992,** 96, 997-1004.
42. Wang, H. F.; Gan, W.; Lu, R.; Rao, Y.; Wu, B. H., *Int. Rev. Phys. Chem.* **2005,** 24, 191-256.
43. Simpson, G. J.; Rowlen, K. L., *J. Am. Chem. Soc.* **1999,** 121, 2635-2636.
44. Long, D. A., *The Raman effect: A unified treatment of the theory of Raman scattering by molecules, John Wiley and Sons* **2002**.
45. Zhang, D.; Gutow, J.; Eisenthal, K. B., *J. Phys. Chem.* **1994,** 98, 13729-13734.
46. Groenzin, H.; Li, I.; Shultz, M. J., *J. Chem. Phys.* **2008,** 128. 214510-8.
47. Allen, M. P.; Tildesley, D. J., *Computer Simulatons of Liquids, Clarendon, Oxford* **1987**.
48. Essmann, U.; Perera, L.; Berkowitz, M. L.; Darden, T.; Lee, H.; Pedersen, L. G., *J. Chem. Phys.* **1995,** 103, 8577-8593.
49. Ryckaert, J. P.; Ciccotti, G.; Berendsen, H. J. C., *J. Comput. Phys.* **1977,** 23, 327-341.
50. Caldwell, J. W.; Kollman, P. A., *J. Phys. Chem.* **1995,** 99, 6208-6219.
51. Wang, J. M.; Wolf, R. M.; Caldwell, J. W.; Kollman, P. A.; Case, D. A., *J. Comput. Chem.* **2004,** 25, 1157-1174.
52. Frisch, M. J. T., G. W.; Schlegel, H. B.; Scuseria, G. E.; Robb, M. A.;; Cheeseman, J. R. M., Jr., J. A.; Vreven, T.; Kudin, K. N.; Burant, J.; C.; Millam, J. M. I., S. S.; Tomasi, J.; Barone, V.; Mennucci, B.; Cossi,; M.; Scalmani, G. R., N.; Petersson, G. A.; Nakatsuji, H.; Hada, M.; Ehara,; M.; Toyota, K. F., R.; Hasegawa, J.; Ishida, M.; Nakajima, T.; Honda, Y.;; Kitao, O. N., H.; Klene, M.; Li, X.; Knox, J. E.; Hratchian, H. P.; Cross, J.; B.; Bakken, V. A., C.; Jaramillo, J.; Gomperts, R.; Stratmann, R. E.;; Yazyev, O. A., A. J.; Cammi, R.; Pomelli, C.; Ochterski, J. W.; Ayala, P. Y.;; Morokuma, K. V., G. A.; Salvador, P.; Dannenberg, J. J.; Zakrzewski, V. G.;; Dapprich, S. D., A. D.; Strain, M. C.; Farkas, O.; Malick, D. K.; Rabuck, A.D.; Raghavachari, K.; Foresman, J. B.; Ortiz, J. V.; Cui, Q.; Baboul, A. G.;; Clifford, S. C., J.; Stefanov, B. B.; Liu, G.; Liashenko, A.; Piskorz, P.;; Komaromi, I. M., R. L.; Fox, D. J.; Keith, T.; Al-Laham, M. A.; Peng, C. Y.;; Nanayakkara, A. C., M.; Gill, P. M. W.; Johnson, B.; Chen, W.;; Wong, M. W. G., C.; and Pople, J. A., *Gaussian 03, Gaussian, Inc.*,

Wallingford CT **2004**.
53. Case, D. A. D., T. A.; Cheatham, III, T. E.; Simmerling, C. L.; Wang, J.;Duke, R. E.; Luo, R.; Merz, K. M.; Wang, B.; Pearlman, D. A.; Crowley, M.; Brozell, S.; Tsui, V.; Gohlke, H.; Mongan, J.; Hornak, V.; Cui, G.; Beroza, P.; Schafmeister, C.; Caldwell, J. W.; Ross, W. S.; Kollman, P.A., *AMBER 8, University of California, San Francisco* **2004**.
54. Forel, M. T.; Tranquil.M, *Spectrochimica Acta Part a-Molecular Spectroscopy* **1970,** A 26, 1023-1034.
55. Covington, A. K.; Thompson, R., *J. Solut. Chem.* **1974,** 3, 603-617.

Table of Contents (TOC) Image

A TOC graphic is required for Articles, Feature Articles, and Review Articles. TOC graphics will appear only in the Web edition of the journal. The illustration should capture the Reader's attention and, in conjunction with the manuscript title, should give the Reader a quick visual impression of the essence of the paper without providing specific results. The graphic should be in the form of a structure, graphical image, photograph, reaction scheme, or equation. The Author must submit the graphic in the actual size to be used for the TOC, fitting in an area 1.375 in. high and 3.5 in. wide (3.6 cm × 8.9 cm). Larger images will be reduced to fit within those dimensions. The type size of labels and other symbols within the graphic must be legible. Tables and spectra are not acceptable. Provide the TOC graphic upon submission of the paper as the last page of the manuscript.